Non-metal photochemical reduction of CO_2 to formate with organohydride-recycle strategy

Weibin Xie,[1] Jiasheng Xu,[1] Ubaidah Md Idros,[1] Jouji Katsuhira,[1] Masaaki Fuki,[1,2] Masahiko Hayashi,[1] Yasuhiro Kobori,[1,2]* Ryosuke Matsubara[1]*

Affiliations
[1]Department of Chemistry, Graduate School of Science, Kobe University, 1-1 Rokkodai-cho, Nada-ku, Kobe 657-8501, Japan. [2]Molecular Photoscience Research Center, Kobe University, 1–1 Rokkodai–cho, Nada–ku, Kobe 657–8501, Japan.

Abstract

The increasing CO_2 concentration in the atmosphere is an urgent social problem that has to be resolved. Reducing CO_2 into compounds useful as energy sources and carbon materials is desirable. For the CO_2 reduction reaction (CO_2RR) to be operational on a global scale, the catalyst system must: (1) use only renewable energy, (2) be built from abundantly available elements, and (3) not require high-energy reactants. Although light is an alluring energy source, most existing methods utilize electricity. Furthermore, catalyst systems are based on rare heavy metals. Herein, we present a transition-metal-free catalyst system for CO_2RR using visible light and containing a carbazole photocatalyst and an organohydride co-catalyst based on benzimidazoline. It produced formate with a turnover number exceeding 8000. No other reduced products such as H_2 and CO were generated, confirming the high selectivity of the system. This finding is essential for operating artificial photosynthesis on a useful scale.

The increase in the atmospheric concentration of greenhouse gas carbon dioxide (CO_2) has become a societal issue; thus, the CO_2 reduction reaction (CO_2RR) is a significant subject as one of the CO_2 fixation processes.[1-4] Although CO_2 is nonpolar molecule, it is chemically reactive because of its polarized C=O double bonds. Carbon dioxide can be reduced electrochemically[5,6] or by using strong reductants or organometallic nucleophiles.[7] However, it is essential to achieve endergonic CO_2RR using renewable energy sources as the input instead of energy sources derived from fossil fuels to render the overall CO_2RR process sustainable and reduce the atmospheric concentration of CO_2.

In this context, photochemical CO_2RR using light, particularly solar energy, as an exclusive external energy source has gained increasing attention. Because the potential of the $CO_2/CO_2^{\bullet-}$ redox couple is considerably negative (E^0 = –2.21 V vs. standard calomel electrode (SCE)), reduction via the single electron transfer (ET) mechanism is difficult (Fig. 1A).[8-10] In contrast, the energetic barrier of CO_2RR via the proton-assisted multi ET mechanism is small (for example, E^0 ($CO_2 + 2H^+ + 2e^- \rightarrow CO + H_2O$) = –0.77 V vs. SCE). Therefore, transition metals such as Co,[11,12] Re, Ru,[13] and Ni,[14] with accessible multiple oxidation states, were used as co-catalysts in most of the previous

studies, in addition to the photocatalysts (PCs). In those cases, the CO_2 coordination with the transition metal co-catalysts enabled the multi-electron CO_2 reduction via the inner-sphere ET mechanism (Fig. 1B).[15] Although a high turnover number (TON) and/or turnover frequency (TOF) were obtained in some cases, the requirement of transition metals became an issue for large-scale practical applications. In addition, kinetically favored production of H_2 by reducing water is a potential competitive pathway in transition metal catalysis, the suppression of which is often formidable.[16]

Formic acid, one of the reduced compounds of CO_2, is a widely used as a reductant, acid, and C1 carbon source in the industry.[17,18] Formic acid and formates are also potent silage ingredients, preservatives, and agrichemicals.[19] Moreover, formic acid and formates can potentially serve as safe liquid organic carriers of hydrogen and energy, thereby attracting attention in mobile vehicle research areas.[20-22] To date, selective generation of formate via photochemical CO_2RR using soluble molecular catalysts has been reported. For example, MacDonnell reported the photochemical reduction reaction of CO_2 to formate using a ruthenium complex and pyridine as a PC and co-catalyst, respectively.[23] Ishitani achieved selective photochemical reduction of CO_2 to formate using a well-designed trinuclear ruthenium complex as a catalyst, wherein a benzimidazoline derivative was used as a stoichiometric terminal reductant.[13,24] Although these examples are of great scientific significance, they rely on the intrinsic capability of transition metals.

In contrast to transition metal complexes, non-metal organomolecules do not have multiple oxidation states or coordination sites for CO_2. Therefore, organomolecules that undergo multi-electron CO_2RR are limited.[25-32] Successful examples are reactions using a combination of frustrated Lewis pairs and metalloid hydride species (B–H or Si–H) (Fig. 1C).[33] However, the issue of low TON and requirement of stoichiometric high-energy metalloid hydride species remains unaddressed. Recently, Musgrave reported that 1,2,3-trimethylbenzimidazoline (**BIH**) reacts with CO_2 to afford formate without the assistance of transition metals or frustrated Lewis pairs (Fig. 1D).[34] This reaction is a groundbreaking example of two-electron CO_2RR achieved exclusively by non-metal organohydrides.[35] Noteworthy in this organomolecular process is the exclusive selectivity in formate formation over H_2 or CO formation. However, a stoichiometric amount of **BIH** was required, and an excess amount (40 equiv to **BIH**) of the metal salt ($NaBF_4$) was used to shift the equilibrium to the product side, which remained obvious tasks to be solved.

Musgrave achieved the regeneration of **BIH** from its oxidized form, 1,2,3-trimethylbenzimidazolium cation ($\mathbf{BI}^+$), via electrochemical reduction, albeit in a vessel separated from the CO_2RR system.[34] We hypothesized that photochemical reduction of $\mathbf{BI}^+$ to **BIH** in the same reaction vessel as CO_2RR could render the CO_2RR system truly catalytic with respect to **BIH** (Fig. 1E). Catalytic reduction of chemicals other than CO_2 with the concept of the *in situ* photochemical regeneration of organohydrides has been developed.[36-44] However, compared to the previous reports that used nicotinamide adenine dinucleotide-mimicking organohydrides, $\mathbf{BI}^+$ had a significantly negative reduction potential (E = –2.12 V vs. SCE), which renders its photochemical reduction challenging. Therefore, benzimidazoline organohydrides have been used as a

stoichiometric reductant to date.[45-49] Furthermore, the dimerization of the organohydride species via its intermediate radical during the regeneration process is another concern.[50] Herein, we report that the visible-light-driven CO_2RR to generate formate based on the concept of *in situ* photochemical organohydride regeneration is viable. The employed PCs were non-metallic small molecules with a high TON of up to 8820 at ambient temperature with 1 atm of CO_2.

(A) *Photocatalytic one-electron reduction of CO_2*

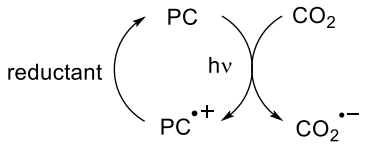

☹ Formidable

(E ($CO_2/CO_2^{\bullet-}$) = –2.21V vs SCE)

(B) *Photocatalytic multi-electron reduction of CO_2*

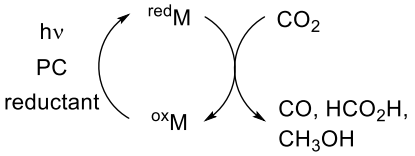

☺ General and precedent

☹ Transition metal catalyst is required.

(M = Ni, Re, Ru, Ir etc)

(C) *Multi-electron reduction of CO_2 with organomolecules and metalloid hydrides*

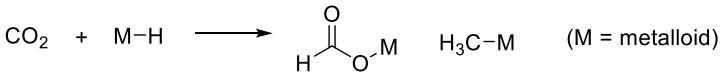

Frustrated Lewis pair (catalytic or stoichiometric)

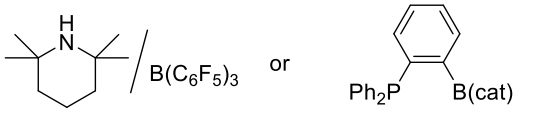

(cat = catecholate)

+

Reductant

Et_3Si-H

B(cat)-H

BH_3-NH_3

☹ Turnover number is low.

☹ Stoichiometric metalloid hydrides are required.

(D) *Two-electron reduction of CO_2 with organohydride*

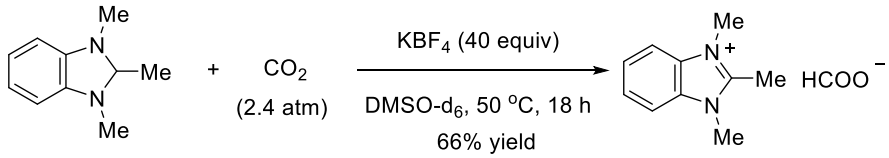

☺ No transition metal is required.

☹ Stoichiometric reaction

(E) *Working hypothesis of present work*

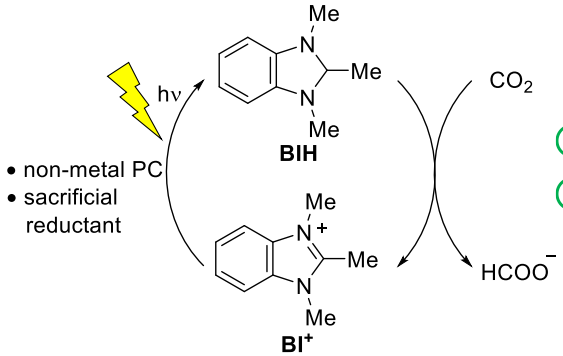

☺ No transition metal is required.

☺ Catalytic for organohydride

Figure 1. Reduction of CO_2 using different strategies. Reported studies (A–D) and present study (E).

Results and Discussion

Photocatalytic CO_2RR

We first investigated the photochemical reduction of $\mathbf{BI}^+$ to determine whether **BIH** can be photochemically recycled. Because $\mathbf{BI}^+$ demonstrates a profoundly negative reduction potential, a PC with a strong reducing capability is required. Conversely, benzimidazoline such as **BIH** is a good electron donor (generally E_{ox} > +0.5 V vs. SCE).[51] The excited state of common PCs readily oxidizes **BIH**, leading to the unproductive consumption of **BIH** and photon. Therefore, a judicious choice of PC is required. Our group focused on developing non-metallic (organic) PCs with high reducing capability. We recently discovered that 3,6-bis(dimethylamino)carbazole molecules could serve as a capable PC with a significantly high reducing capability in its excited state (up to E^* = –2.75 V vs. SCE). This class of carbazoles is characterized by a red-shifted absorption of approximately 80 nm as compared to the parent carbazole, and absorbs visible light.[52,53] The photocatalytic reduction of $\mathbf{BI}^+(\mathbf{I}^-)$ to its reduced-state **BIH** employing **1** as a PC remarkably proceeded in 44% yield under visible light irradiation (400 nm) in a water-containing solvent system in the presence of ascorbic acid ($\mathbf{H_2A}$) as a sacrificial reductant (Fig. 2). The mass balance of this reaction was almost quantitative, suggesting that both $\mathbf{BI}^+$ and **BIH** have sufficient stability to be competent for long-term catalytic performance.

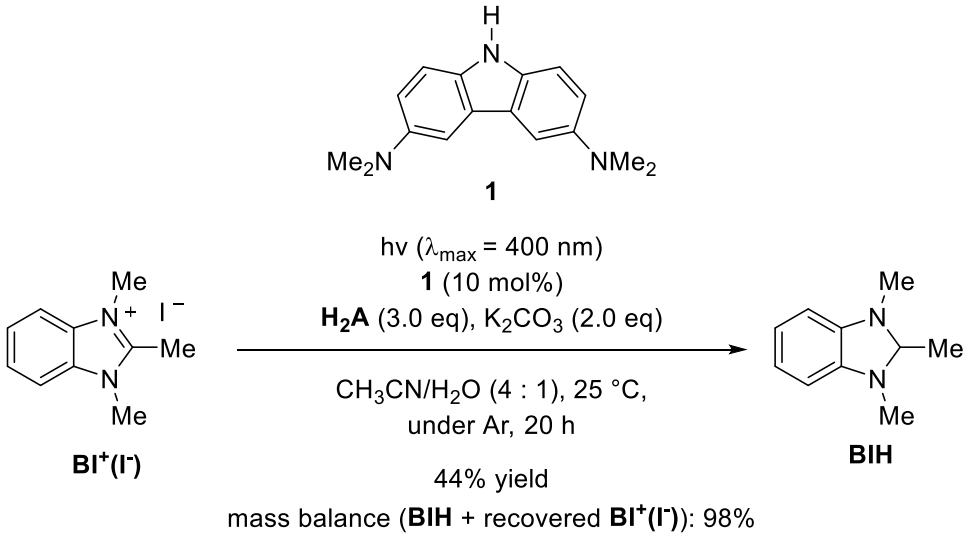

Figure 2. Reduction of $\mathbf{BI}^+$ to **BIH** via visible light-driven photoreaction.

With the promising data obtained for the photochemical regeneration of **BIH**, we next investigated the photochemical CO_2RR using a catalytic amount of **BIH**. Entry 1 of Table 1 illustrates the developed procedure. Formate was obtained as a CO_2-reduced product, with a yield of 143% (100 × the amount of formate formed (mol)/the amount of employed sacrificial reductant (mol)), which was revealed by proton nuclear magnetic resonance (^{1}H NMR) analysis. To the best of our knowledge, this is the first

example of a visible-light-driven photocatalytic CO_2RR to generate any reduced C1 product using a non-metallic small molecular catalyst. The observed yield of more than 100% indicates that **H_2A** donates more than two electrons, which will be discussed later. Methanol, formaldehyde, and oxalate were not detected as a product by ^{1}H NMR or carbon-13 NMR (^{13}C NMR) analysis of the solution phase (Fig. S2). The gas chromatography (GC) analysis of the reactor headspace revealed that the evolution of gaseous products, CO or H_2, was below the detection limit (0.1% and <0.8% yield for H_2 and CO, respectively) (Fig. S3 and S4). Thus, our protocol for CO_2RR exhibits exclusive selectivity to afford formate as the sole product, which contrasts the previous transition metal-catalyzed CO_2RR, where concomitant H_2 generation is often an issue. The quantum yield of CO_2RR was 6.5% (Fig. S7).

Base, light irradiation, **H_2A**, and PC **1** are indispensable in this reaction, as revealed by control experiments (Table 1, entries 2–6). The yield dropped to 8% (entry 7) without **$BI^+(I^-)$**, suggesting its importance as a catalyst. Consistent with the working hypothesis, the use of **BIH** instead of **$BI^+(I^-)$** gave comparable results (entry 8 vs. entry 1). This result indicates that iodide anions are not involved in the catalytic cycle. In addition, K_2CO_3 was replaced with other inorganic salts (entries 9–14), implying that the type of counter cations and basic anions moderately affects the reaction. In entries 15 and 16, inorganic sacrificial reductants, Na_2SO_3 and $NaHSO_3$, were used instead of **H_2A**, resulting in 64% and 61% yields, respectively. Although the yields were lower than that of entry 1, Na_2SO_3 and $NaHSO_3$ were capable reductants because they donated two electrons per molecule (the maximum product yield is 100%). Formate was generated even without CO_2 gas in the presence of K_2CO_3 (entry 17); however, minimal formate was generated without CO_2 gas or K_2CO_3 (entry 18), suggesting that CO_3^{2-} could serve as a source of CO_2 in the present system. Next, the PCs were screened (entries 19–25, Fig. 3). Carbazole-based organic PCs with electron-withdrawing groups did not generate formate (entries 19–21) due to the insufficient reducing capability of the excited states of these PCs to transfer an electron to **BI^+**. PC **5**, with electronic feature similar to that of **1**, gave a comparable formate yield of 127% (entry 22). Tris(2-phenylpyridinato)iridium (III) or $Ir(ppy)_3$ (**7**) could also serve as a competent PC, affording formate in 132% yield (entry 24). Without **$BI^+(I^-)$**, $Ir(ppy)_3$ did not afford formate, suggesting that the $Ir(ppy)_3$-catalyzed CO_2RR proceeded via a **$BI^+(I^-)$**-involving mechanism, similar to the reaction using **1**. Thus, the catalyst combination of $Ir(ppy)_3$ and **$BI^+(I^-)$** was unprecedented and a new discovery in the present study. Tris(2,2'-bipyridyl)ruthenium (II) chloride hexahydrate or $Ru(bpy)_3Cl_2\bullet 6H_2O$ (**8**) did not promote the reaction (entry 25).

Table 1. Photocatalytic CO_2 reduction reaction.

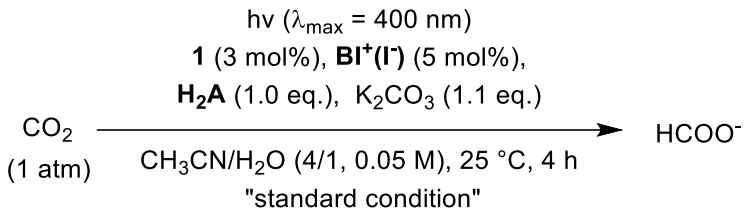

Entry	Variation from above "standard condition"	Yield/%[a]
1	None	143
2	Without K_2CO_3	0
3	KCl (2.0 eq) instead of K_2CO_3	<1
4[b]	No light	0
5[b]	Without **H_2A**	<1
6	Without **1**	0
7	Without **$BI^+(I^-)$**	8
8	**BIH** instead of **$BI^+(I^-)$**	142
9	Li_2CO_3 (1.1 eq) instead of K_2CO_3	68
10	Na_2CO_3 (1.1 eq) instead of K_2CO_3	114
11	Cs_2CO_3 (1.1 eq) instead of K_2CO_3	122
12	KOH (2.2 eq) instead of K_2CO_3	78
13	NaOH (2.2 eq) instead of K_2CO_3	103 (117)[b]
14	K_3PO_4 (2.2 eq) instead of K_2CO_3	143
15	Na_2SO_3 instead of **H_2A**	64 (52)[c]
16	$NaHSO_3$ instead of **H_2A**	61 (3)[c]
17	Argon instead of CO_2	104
18	Argon instead of CO_2, NaOH (2.2 eq) instead of K_2CO_3	5
19	**2** instead of **1**	0
20	**3** instead of **1**	0
21	**4** instead of **1**	0
22	**5** instead of **1**	127
23	**6** instead of **1**	111
24	**7** instead of **1**	132 (0)[d]
25	**8** instead of **1**	0

[a] 100 × the amount of formate formed (mol)/the amount of employed sacrificial reductant (mol)

[b] Reaction time: 20 h

[c] Without K_2CO_3

[d] Without **$BI^+(I^-)$**

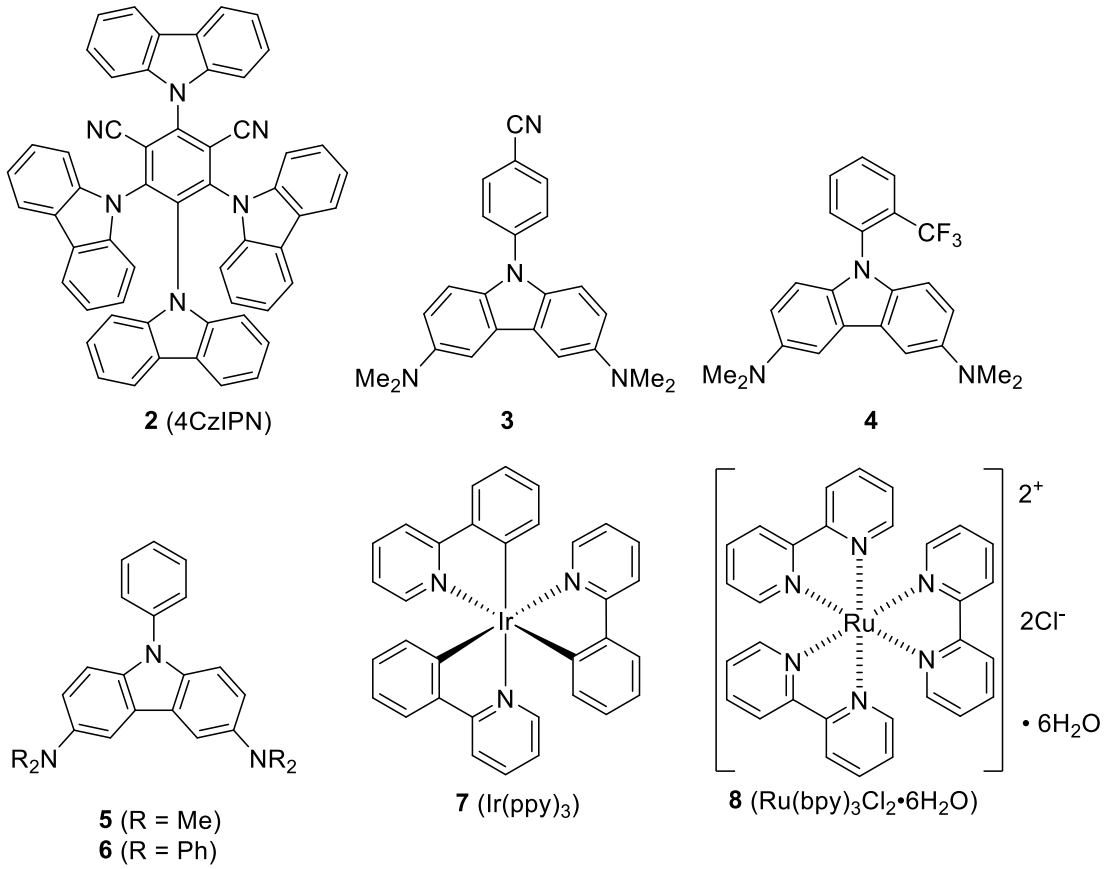

Figure 3. Employed photocatalysts.

We utilized $^{13}CO_2$ instead of $^{12}CO_2$ (Fig. 4A) to confirm that the singlet peak at 8.8 ppm in ^{1}H NMR spectrum was assigned to formate, thereby confirming that the carbon source of formate was derived from CO_2. Sodium hydroxide was used as the base to avoid contaminating $^{12}CO_2$ derived from K_2CO_3 (Table 1, entry 17). ^{1}H NMR analysis revealed that ^{13}C-formate, characterized by a set of doublet peaks ($^1J_{CH}$ = 192.8 Hz), was obtained in 90% yield, along with a 3% yield of ^{12}C-formate (Fig. 4B). The formation of ^{12}C-formate is ascribed to $^{12}CO_2$ released from **H₂A** (vide infra, Fig. 6). In the ^{13}C NMR spectrum of the same reaction, an intense ^{13}C-formate at 169.4 ppm was observed (Fig. 4C). These results demonstrate that the main carbon source of the product formate is gaseous CO_2 introduced exogenously.

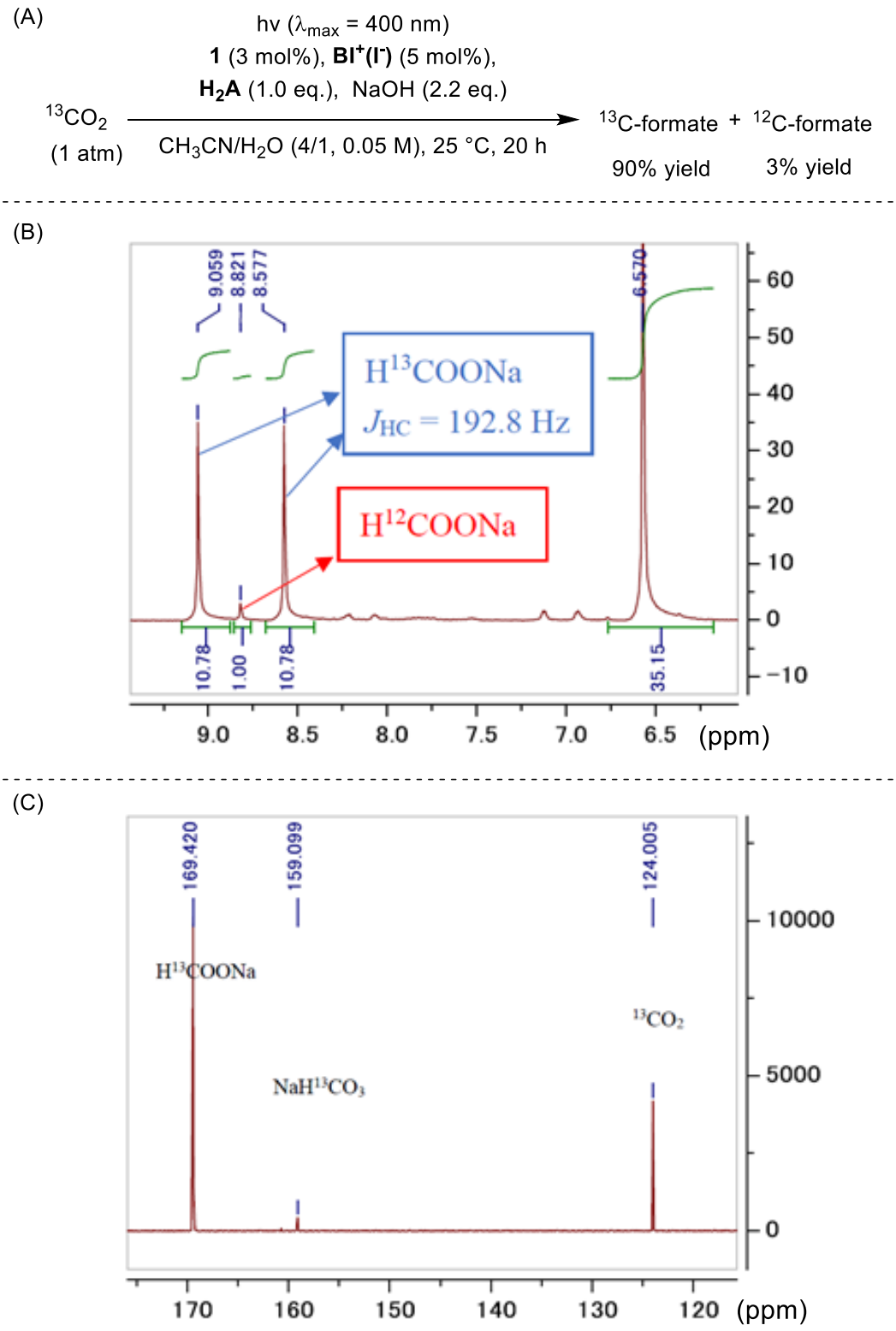

Figure 4. Carbon-13 (^{13}C)-labeling experiment. (A) Reaction conditions. (B) Proton nuclear magnetic resonance (^{1}H NMR) spectrum of the reaction mixture. The singlet peak at 6.57 ppm is trimethoxybenzene (internal standard). (C) ^{13}C NMR spectrum of the reaction mixture.

Next, we focused on developing catalysts with carbazole and **BI**$^{+}$ moieties in one

molecule. We designed **9**, **10**, and **11** to probe the conceptual feasibility of the presumed all-in-one catalyst. The carbazole and **BI**$^+$ moieties were covalently connected by the alkyl-chain linkers in **9** and **10**, while **11** was the reduced form of **10** (Fig. 5). The synthesis of these molecules is illustrated in Fig. S8. The absorption spectra of **9** and **10** are similar to the average of those of **1** and **BI**$^+$ added together, suggesting no significant electronic interaction between the carbazole and benzimidazolium parts in the ground state (Fig. S9). Visible light-driven CO_2RR using 1 mol% of all-in-one catalysts **9**, **10**, and **11** provided formate in 72, 68, and 56% yields, respectively (Table S1). These data proved that photochemical CO_2RR using a single molecular catalyst is conceptually viable. The observed moderate catalytic activity of **9**–**11** is ascribed to the unproductive back ET; further optimization of the catalyst structure is required.

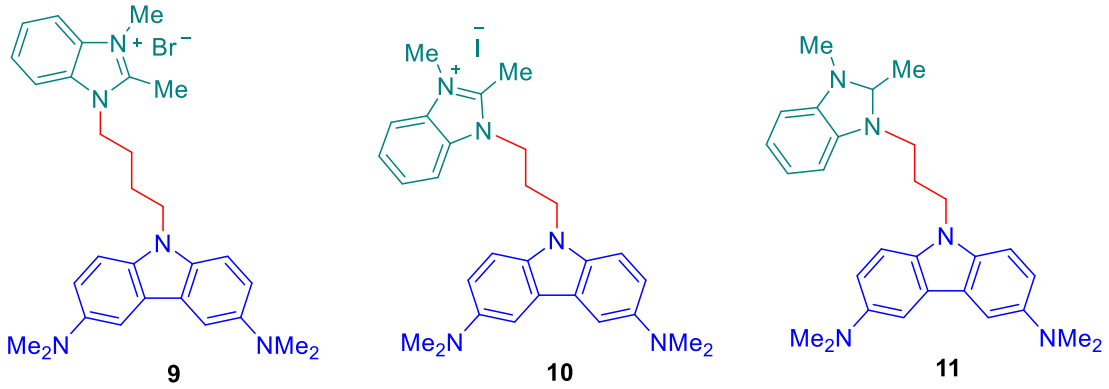

Figure 5. Structures of all-in-one photocatalysts.

TON and TOF are parameters used to evaluate the durability and kinetic activity of the catalyst. Higher TON and TOF for the potential PCs (**1**, **5**, **6**, and **7**) were sought for the developed CO_2RR using 0.01 mol% of PC and 5 mol% of **BI**$^+$**(I**$^-$**)** at 4 h reaction time (Table 2, entries 1–4). Using organic PC **6**, TON and TOF reached 8820 and 2205 h^{-1}, respectively (entry 3). TON and TOF for **BI**$^+$**(I**$^-$**)** were 6070 and 1520 h^{-1}, respectively using 1 mol% of PC **5** and 0.01 mol% of **BI**$^+$**(I**$^-$**)** (entry 6). These large values indicate that the employed PCs and **BI**$^+$**(I**$^-$**)** have high durability and activity for CO_2RR. The catalyst loadings of both PC **5** and **BI**$^+$**(I**$^-$**)** could be simultaneously reduced to 0.1 mol% (entry 8), while further decreasing the catalyst loading led to low yields (entries 9 and 10).

Table 2. Investigation on the decrease of the catalyst loading.

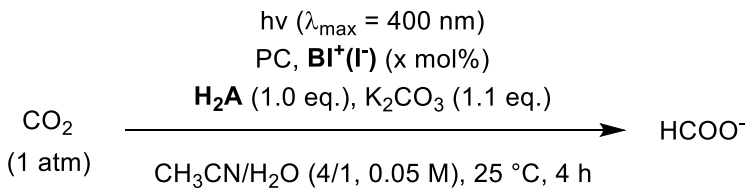

Entry	Photocatalyst (PC)	x	Yield /%[a]	TON (PC/ **BI**$^+$**(I**$^-$**)**)	TOF /h (PC/ **BI**$^+$**(I**$^-$**)**)
1	**1** (0.01 mol%)	5	27	**2750**/5	**687**/1

2	**5** (0.01 mol%)	5	65	**6510**/10	**1630**/2
3	**6** (0.01 mol%)	5	88	**8820**/18	**2205**/5
4	**7** (0.01 mol%)	5	74	**7380**/15	**1845**/4
5	–	5	0	–	–
6	**5** (1 mol%)	0.01	61	61/**6070**[b]	15/**1520**[b]
7	**5** (1 mol%)	0	9	–	–
8	**5** (0.1 mol%)	0.1	71	**710**/**710**	**178**/**178**
9	**5** (0.01 mol%)	0.1	9	860/86	215/22
10	**5** (0.01 mol%)	0.01	0	–	–

[a] 100 × the amount of formate formed (mol)/the amount of employed **H_2A** (mol)

[b] Values calculated without considering the background reaction and proceeding without the involvement of **$BI^+(I^-)$** (entry 7).

Mechanistic Study

Investigating the role of H_2A

In some photocatalytic CO_2RRs using **H_2A** as a sacrificial reductant (for example entry 1 in Table 1), the yields based on the loading of **H_2A** exceeded 100%, assuming that **H_2A** is a two-electron donor. This result implies that **H_2A** releases more than two electrons per molecule. The proposed pathway for the conversion of **H_2A** is shown in Fig. 6. After releasing two electrons, **H_2A** was converted to dehydroascorbic acid (**A**). Delactonization of **A** yielded **12**, which was converted to aldehyde **13** with the release of CO_2. Further, **13** underwent deprotonation to form **14**, which was a potential electron donor because it has an enediol structural motif analogous to **H_2A**.[54] A commercially available **A** was used instead of **H_2A** in the photocatalytic CO_2RR to verify the above hypothesis (Table 3, entry 2). Formate was obtained in 74% yield, corroborating the hypothesis that **A** also served as a reductant. Next, $^{13}CO_2$ was used instead of $^{12}CO_2$ under identical conditions (entry 3). As a result, 17% and 45% of ^{12}C- and ^{13}C-formate was yielded, respectively. Formate was obtained in 30% yield even without CO_2 gas (entry 4). Two possible pathways were suggested to explain these results: path (1): **A** degraded to CO_2, which was converted to formate in the photocatalytic cycle of CO_2RR, and path (2): **A** directly degraded to formate. Several control experiments were conducted to clarify the plausible mechanism (entries 5–7). No formation of formate without **$BI^+(I^-)$** (entry 5) strongly supported path (1). The omission of base or **1**, both indispensable in photocatalytic CO_2RR, did not form formate, which was also consistent with path (1). Thus, the following conclusions are drawn: (a) According to the proposed mechanism shown in Fig. 6, **H_2A** can operate as a four-electron donor; (b) **H_2A** releases CO_2 during its oxidation, which can be a carbon source of formate; (c) direct generation of formate derived from the degradation of **H_2A** is implausible.

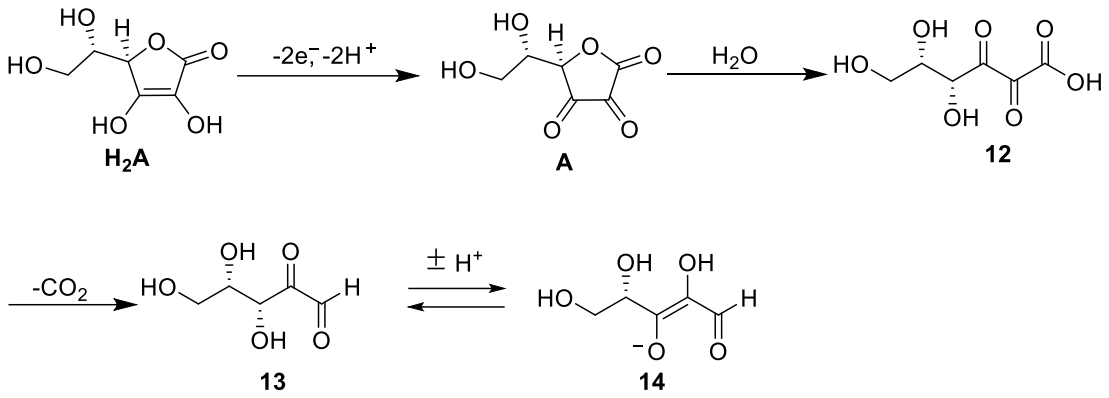

Figure 6. Proposed mechanism for the conversion of **H_2A**.

Table 3. Utilization of **A** as a sacrificial reductant.

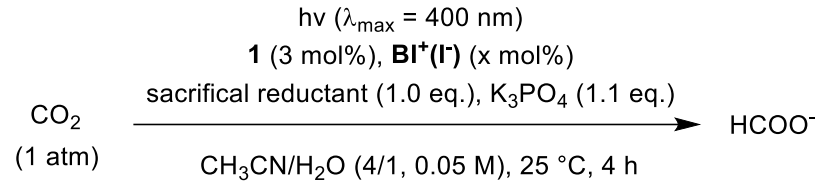

Entry	Sacrificial reductant	CO_2	Yield/%[a]
1[b]	**H_2A**	$^{12}CO_2$	143
2	**A**	$^{12}CO_2$	74
3	**A**	$^{13}CO_2$	45 (^{13}C-formate) 17 (^{12}C-formate)
4	**A**	Not used	30
5[c]	**A**	Not used	0
6[d]	**A**	Not used	0
7[e]	**A**	Not used	0

[a] 100 × the amount of formate formed (mol)/the amount of employed sacrificial reductant (mol)

[b] K_3PO_4 (2.2 eq) was used

[c] Without **$BI^+(I^-)$**

[d] Without K_3PO_4

[e] Without **1**

Mechanism for photosensitization

Next, we focused on the organohydride regeneration mechanism. Light irradiation was required for CO_2RR (Table 1, entry 4). Because **$BI^+(I^-)$** did not demonstrate absorption at 400 nm (Fig. S9), the excitation of PC carbazole initiated photosensitization. We performed experiments to gain insight into the mechanism of the initial photosensitization. For the following experiments, **1** or **5** was used as a representative PC. First, the formation of an electron donor-acceptor (EDA) complex between PC **1** and **$BI^+(I^-)$** was explored by measuring the steady-state ultraviolet-visible absorption of the mixed solution (Fig. S11). No new peak was observed compared to

the original spectrum of each compound, suggesting that no EDA complex was generated. The existence of the exciplex was improbable because the normalized emission spectra of PC **1** in the presence and absence of **BI$^+$(I$^-$)** were identical (Fig. S12). We further examined the involvement and influence of the excited states (singlet or triplet) of PC in reducing **BI$^+$(I$^-$)**. Thus, the rate constants of fluorescence quenching (k_q) of PC **1** by **BI$^+$(I$^-$)** and ascorbate anion (**HA$^-$**) were determined according to the Stern-Volmer equation, $I_0/I = 1 + k_q \cdot \tau_0 \cdot [Q]$, where I_0 and I represent the fluorescence intensity in the absence and presence of the different concentrations of the quencher, respectively; τ_0 represents the lifetime of the excited state of PC; [Q] is the quencher concentration. The time-resolved fluorescence measurement of PC **1** yielded a value of τ_0 of 19.2 ns (Fig. S13). The results of the ET fluorescence quenching of PC **1** in the presence of varying concentrations of **BI$^+$(I$^-$)** as a quencher are illustrated in Fig. 7. Therefore, the k_q by **BI$^+$(I$^-$)** had a value of 2.71×10^9 mol L^{-1} s^{-1}, indicating that a single ET from the excited **1** to **BI$^+$(I$^-$)** occurred efficiently. In contrast, fluorescence quenching of **1** by **HA$^-$** was not observed (Fig. 7). Thus, an oxidative quenching cycle was suggested. The fluorescence quantum yield Φ_{fl} and lifetime τ_0 of **1**, **9**, **10**, and **11** are listed in Table S3. The values of Φ_{fl} and τ_0 of **9** and **10** were two orders of magnitude lower than those of **1**, while **11** had values of Φ_{fl} and τ_0 similar to those of **1**. In addition, these results suggested that the singlet excited state of the carbazole moiety underwent a single ET to the benzimidazolium cation.

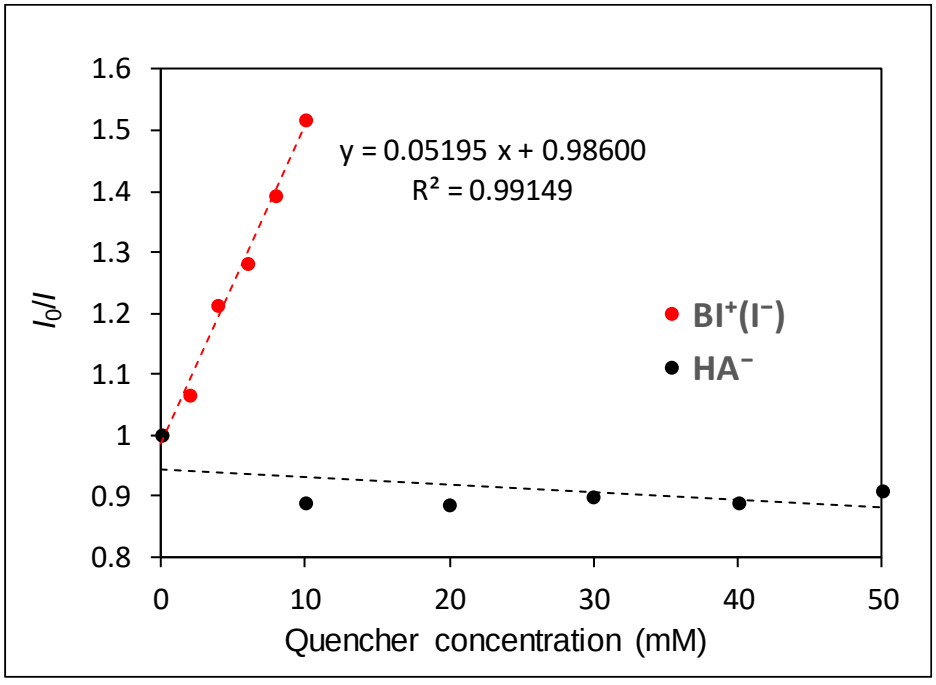

Figure 7. Fluorescence quenching of photocatalyst **1** in the presence of varying concentrations of **BI$^+$(I$^-$)** or **HA$^-$** as quenchers. Solvent: DMSO for **BI$^+$(I$^-$)**, CH_3CN/H_2O (1/1 v/v) for **HA$^-$**. The concentration of **1**: 1.0×10^{-5} mol L^{-1}. The ratios of fluorescence intensities at 450 nm in the presence (I) and absence (I_0) of the quenchers are represented by the function of the quencher concentrations.

Although the involvement of the singlet excited state of PC in reducing **BI$^+$(I$^-$)** was evident, the involvement of the triplet excited state of PC could not be excluded. Therefore, we experimentally characterized the optoelectronic properties of PC **5** and **BI$^+$(I$^-$)** (Fig. S17–S19). The results are summarized in Table 4. The oxidation potential of the singlet excited state of **5** (hereafter denoted as ^{1}**5***) was E (**5**$^{\bullet+}$/^{1}**5***) = –2.65 V vs. SCE. The obtained oxidation potential was more negative than the reduction potential of **BI$^+$(I$^-$)** (E_{red} = –1.96 V vs. SCE), suggesting that the ET from ^{1}**5*** to **BI$^+$(I$^-$)** was possible. These results are consistent with those of the Stern-Volmer experiments. The oxidation potential of the triplet excited state of **5** (hereafter denoted as ^{3}**5***) was E (**5**$^{\bullet+}$/^{3}**5***) = –2.30 V vs. SCE. Additionally, the ET from ^{3}**5*** to **BI$^+$(I$^-$)** was exothermic with ΔG_{CS} = –0.34 eV, where ΔG_{CS} is the Gibbs free energy change for charge separation. The triplet state energies (E_T) of **5** and **BI$^+$(I$^-$)** were 2.64 and 3.02 eV, respectively, deducing that the triplet energy transfer was endothermic from ^{3}**5*** to **BI$^+$(I$^-$)**.

Table 4. Optoelectronic data of **5** and **BI$^+$(I$^-$)**.

	E_S /eV	E_T /eV	E_{ox} (vs SCE)	E_{red} (vs SCE)	$^1E_{ox}$* (vs SCE)	$^3E_{ox}$* (vs SCE)
5	2.99	2.64	0.34	-2.75	-2.65	-2.30
BI$^+$(I$^-$)	4.22[a]	3.02	(0.31)[b]	-1.96	–	–

Es, E_T: singlet and triplet state energies approximated as the high-energy onset of fluorescence and phosphorescence spectra, respectively, where the emission intensity is 10% of the obtained at the maximum emission wavelength.[55,56]

E_{ox}, $E_{red:}$ oxidation and reduction potentials of the ground state of molecules obtained from cyclic voltammetry analysis, respectively. When reversible cyclic voltammograms were obtained, standard reduction potentials (E^0) were calculated by averaging the forward and reverse peak potentials. When irreversible cyclic voltammograms were obtained, half-peak potentials ($E_{p/2}$), corresponding to the potential at half the maximum current of the cyclic voltammogram, were used as an estimate of E^0.[57]

$^1E_{ox}$*, $^3E_{ox}$*: oxidation potential of the singlet and triplet excited states of molecules, respectively, calculated using the Rehm-Weller equation.[58]

[a]The value of **BI$^+$(BF$_4^-$)** is presented because **BI$^+$(I$^-$)** demonstrated phosphorescence instead of fluorescence even at 293 K due to the heavy atom effect.

[b]This value was ascribed to iodide oxidation.

The detection of the radical cation of PC **5** was attempted by transient absorption spectroscopy to directly confirm that the ET event occurs via the excited states of **5**. As a preliminary step, **5**$^{\bullet+}$ was chemically generated by treating **5** with an equimolar amount of magic blue, a single electron oxidant (E_{red} = +1.1 V vs. SCE),[59] and the steady-state absorption spectrum of **5**$^{\bullet+}$ was measured (Fig. 8, red line). The absorption bands at 470, 550, 700, and >1100 nm (marked with black arrows) were assigned to **5**$^{\bullet+}$ (Fig. S20), which was corroborated by the time-dependent density functional theory (TD-DFT) calculations (Table S4); the calculated wavelength of the absorption peaks

(Fig. 8, orange bars) matched the experimental spectra. After obtaining the authentic absorption spectrum of $\mathbf{5}^{\bullet+}$, the transient absorption of the solution of **5** in the presence of $\mathbf{BI}^{+}\mathbf{(I}^{-}\mathbf{)}$ was measured (Fig. 9). Long-lived absorption bands with millisecond decay were observed at 470, 550, and 700 nm. These bands were assigned to $\mathbf{5}^{\bullet+}$ generated via ET from the excited state of **5** to $\mathbf{BI}^{+}\mathbf{(I}^{-}\mathbf{)}$, although they could partially contain the absorption of $\mathbf{BI}^{\bullet}$, which was predicted to appear at 560 nm by the TD-DFT calculation (Fig. 8, blue bars). The time profile analysis of the absorption bands revealed that the observed millisecond decays were not exponential and obeyed total second-order kinetics (Fig. 10 and 11); thus, they were attributed to the bimolecular charge-recombination reactions between $\mathbf{5}^{\bullet+}$ and $\mathbf{BI}^{\bullet}$. The time profiles of the absorbance changes in the region of microseconds manifested a quick decay component at 700 nm (Fig. 12). This decay was attributed to the T_1-T_n absorption of **5** (Fig. S21–S23), with a lifetime of 1.1 μs in the presence of $\mathbf{BI}^{+}\mathbf{(I}^{-}\mathbf{)}$. The lifetime of $^{3}\mathbf{5}^{*}$ in the absence of $\mathbf{BI}^{+}\mathbf{(I}^{-}\mathbf{)}$ was 0.89 μs (Fig. S23). Because the lifetime of $^{3}\mathbf{5}^{*}$ was not significantly affected by the addition of $\mathbf{BI}^{+}\mathbf{(I}^{-}\mathbf{)}$, the ET or energy transfer from $^{3}\mathbf{5}^{*}$ to $\mathbf{BI}^{+}\mathbf{(I}^{-}\mathbf{)}$ was not the major pathway for reducing benzimidazolium cations. The lack of triplet quenching by the ET pathway suggests $k_q < 10^7$ mol L^{-1} s^{-1} as the bimolecular rate constant between $^{3}\mathbf{5}^{*}$ and $\mathbf{BI}^{+}$ for the small exothermicity of $-\Delta G_{CS} = 0.34$ eV. This smaller rate constant than $k_q = 2.71 \times 10^9$ mol L^{-1} s^{-1} for the $^{1}\mathbf{5}^{*}$-precursor case ($-\Delta G_{CS} = 0.69$ eV) is explained by large reorganization energy exceeding 1 eV, which is consistent with the solvent reorganization energy in highly polar solvents such as acetonitrile and DMSO. In conclusion, the reduction of $\mathbf{BI}^{+}\mathbf{(I}^{-}\mathbf{)}$ to **BIH** is initiated by the ET from $^{1}\mathbf{5}^{*}$ to $\mathbf{BI}^{+}\mathbf{(I}^{-}\mathbf{)}$.

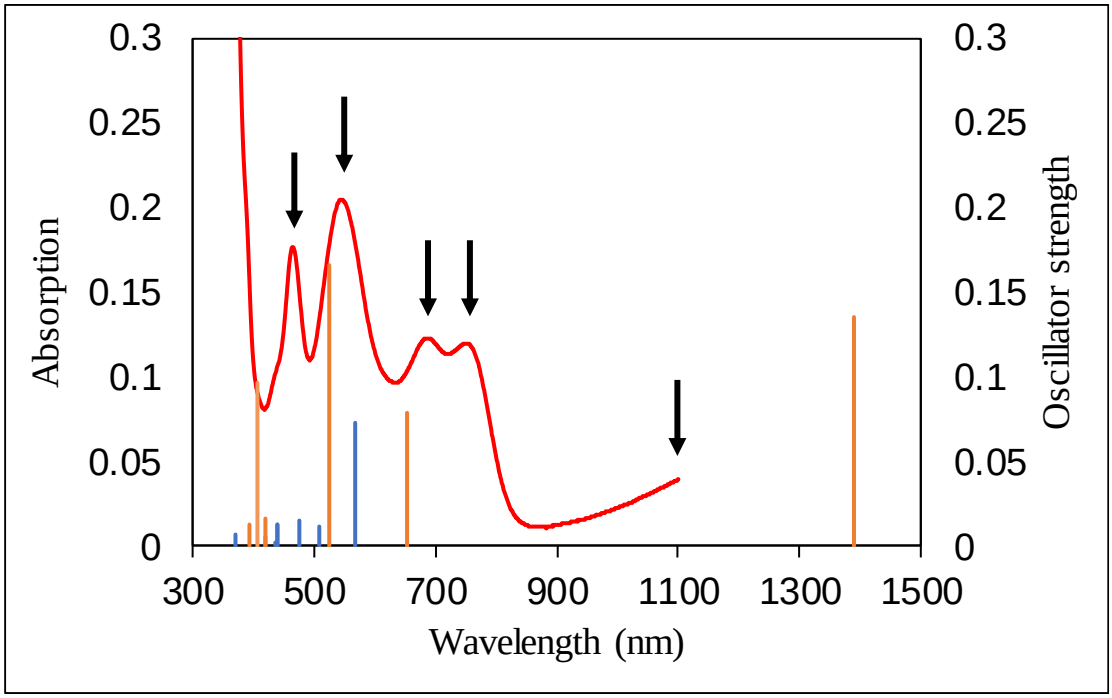

Figure 8. The absorption of $\mathbf{5}^{\bullet+}$ (red line) and the calculated oscillator strength of $\mathbf{5}^{\bullet+}$ (orange bar) and $\mathbf{BI}^{+}\mathbf{(I}^{-}\mathbf{)}$ (blue bar). $\mathbf{5}^{\bullet+}$ was generated by treating **5** (100 μM) with magic blue (100 μM) in CH_2Cl_2. The oscillator strengths were calculated by the time-dependent density functional theory (TD-DFT) method at the B3LYP/6-

31++G(d,p)/CPCM (DMSO) level based on the geometries optimized by the DFT method at the ULC-BLYP/6-31++G(d)/CPCM(DMSO) level.

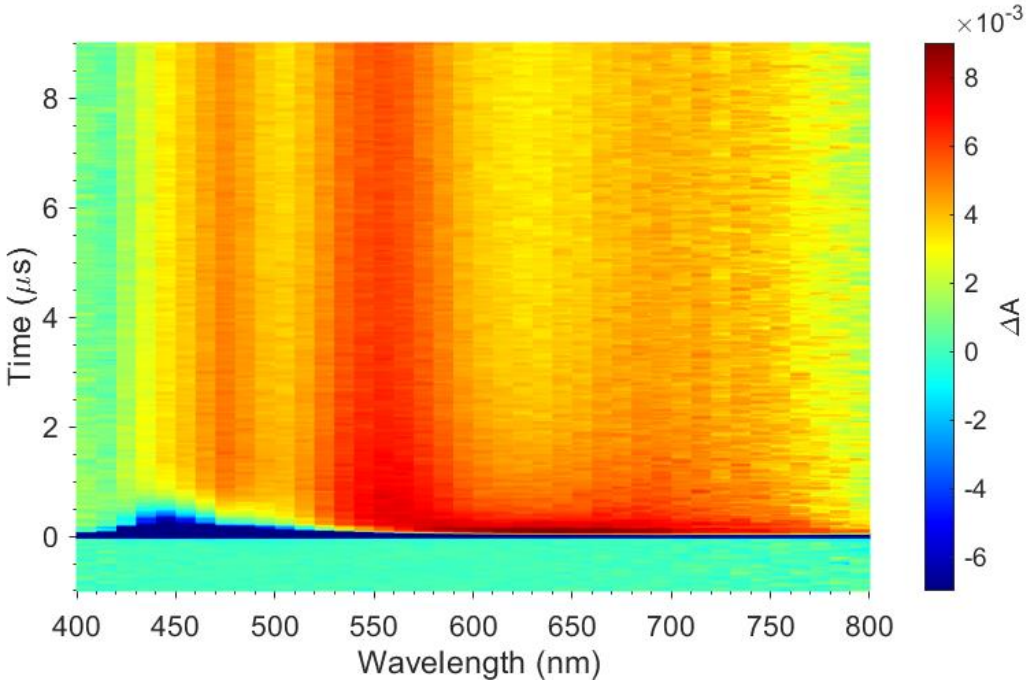

Figure 9. Two-dimensional data of the absorbance change (transient absorption) obtained by the laser irradiation of 355 nm of the DMSO solution of **5** (0.2 mM) in the presence of **BI$^+$(I$^-$)** (30 mM) at 293 K. The long-lived absorption bands were observed at 470, 550, and 700 nm and are assigned to the transient absorption composed of **5$^{\bullet+}$** and **BI$^\bullet$**, a one-electron reduced form of **BI$^+$**.

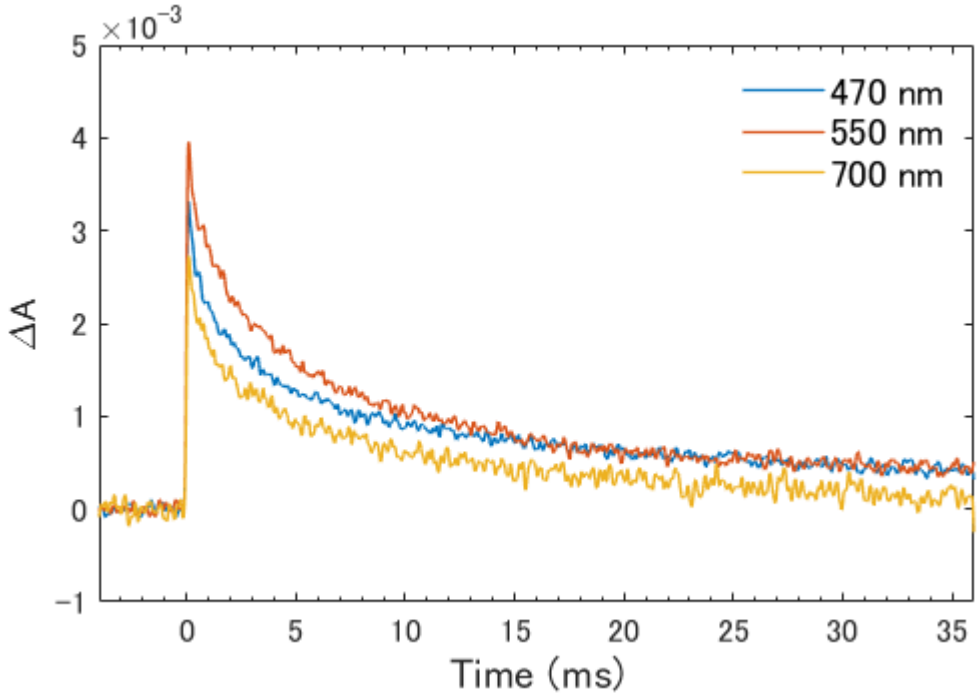

Figure 10. Time profiles of the absorbance changes obtained in Fig. 9 from the delay

time of 0 ms to 35 ms. These non-exponential decays obey a second-order kinetics as shown in Fig. 11.

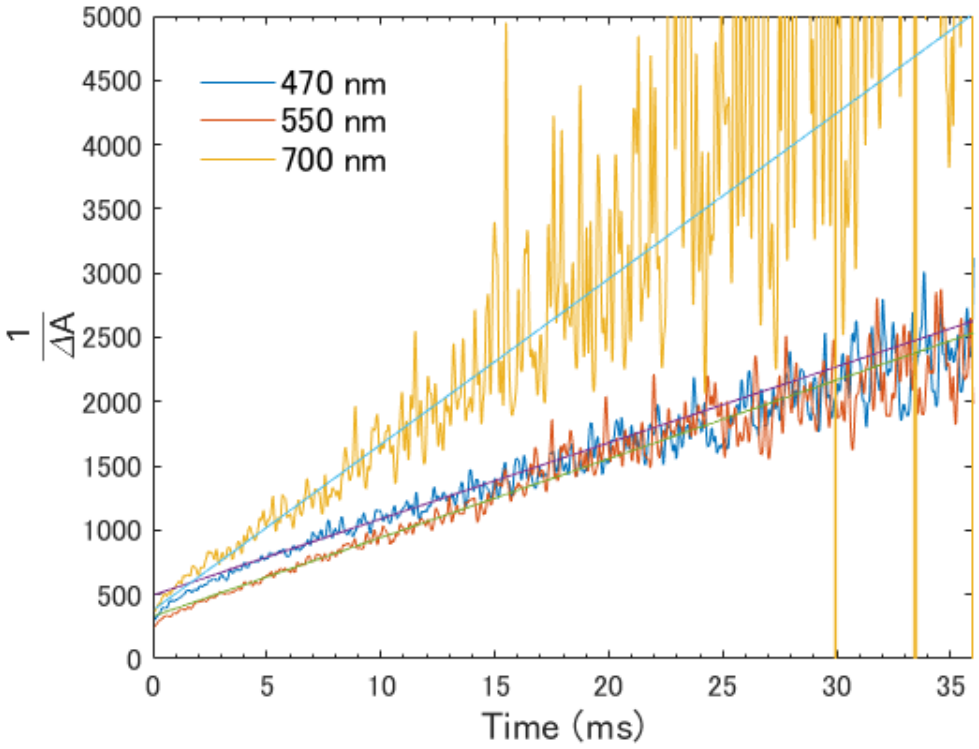

Figure 11. Time profiles of the inverse values ($1/\Delta A$) of the absorbance changes obtained from Fig. 10. This dependence of the decay on the second-order kinetics is attributed to the bimolecular charge-recombination reaction between $\mathbf{5}^{\bullet+}$ and $\mathbf{BI}^{\bullet}$.

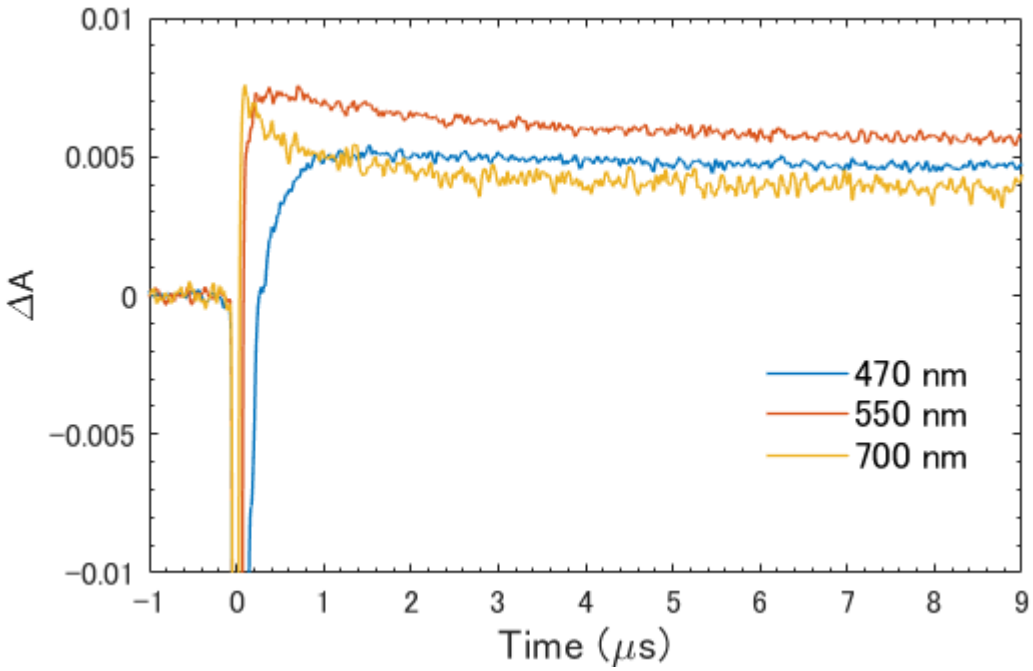

Figure 12. Time profiles of the absorbance changes obtained in Fig. 9 from 0 μs to 9

μs delay time. At 700 nm, the quick decay component corresponds to T_1-T_n absorption of **5**, which decay lifetime was obtained to be 1.1 μs. The lifetime of ^{3}**5*** (0.89 μs obtained in Fig. S23) was not affected by the addition of **BI$^+$(I$^-$)** but by the triplet-triplet annihilation, denoting that the ET or energy transfer from ^{3}**5*** to **BI$^+$(I$^-$)** is not the major pathway for the reduction of benzimidazolium cation.

Mechanism for converting BI$^\bullet$ to BIH

After confirming the possible influence of ET in the initial photochemical step, we examined the mechanism for converting the photochemically generated **BI$^\bullet$** to BIH. The electrochemical conversion from **BI$^+$** to **BIH** via **BI$^\bullet$** was thoroughly investigated by Lim et al.[34] Two pathways were initially proposed with respect to the conversion of **BI$^\bullet$** to **BIH**: ET followed by proton transfer (PT) and PT followed by ET. Based on the results that (1) the irreversible reduction of **BI$^+$** was observed in the absence of acid, which was ascribed to the dimerization of **BI$^\bullet$** and (2) the current intensity of the first reduction wave increased in the presence of acid, Lim et al. concluded that **BI$^\bullet$** underwent PT to generate **BIH$^{\bullet+}$**, followed by ET to give **BIH**. In our reaction (Fig. 13), the PT to **BI$^\bullet$** is unlikely based on the employed basic condition and low acidity of **BIH$^{\bullet+}$** (pK_a = 15.4 in DMSO).[50] Conversely, the ET from ^{1}**5*** (E (**5**$^{\bullet+}$/^{1}**5***) = –2.65 V vs. SCE) to **BI$^\bullet$** (E (**BI$^\bullet$**/**BI$^-$**) = –2.42 V vs. SCE) is exothermic. However, both ^{1}**5*** and **BI$^\bullet$** are transient species with short lifetimes in low-concentration catalytic amounts, making the ET difficult before dimerization of **BI$^\bullet$**. Alternatively, we examined the possibility of hydrogen atom transfer (HAT), a process wherein protons and electrons are transferred simultaneously. The enthalpy change of HAT from **HA$^-$** or **HA$^\bullet$** to **BI$^\bullet$** is largely negative (ΔH^o = –31.1 or –25.4 kcal/mol, respectively), thus more plausible channel for converting **BI$^\bullet$** to **BIH** has been identified.[60]

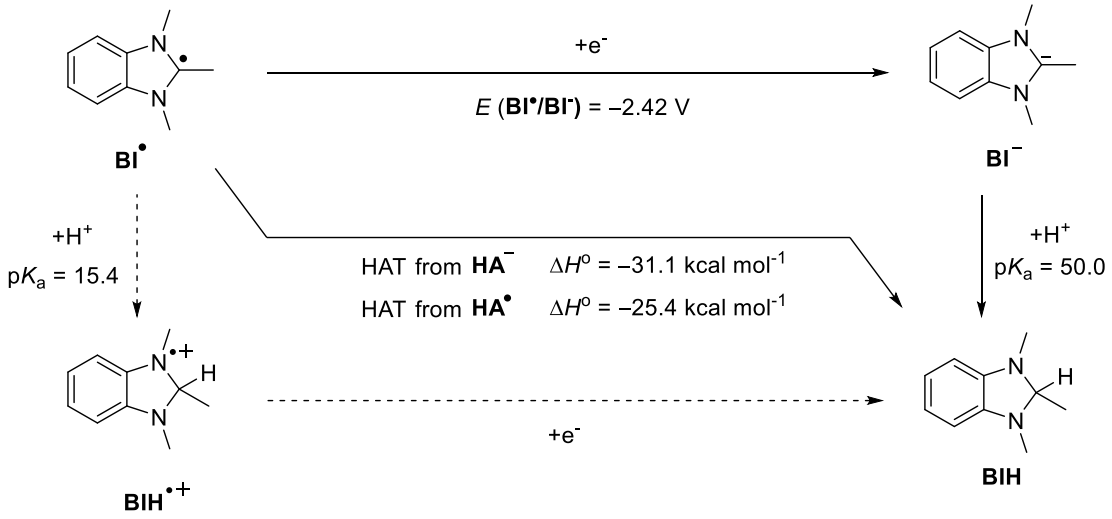

Figure 13. Pathway for the conversion of **BI$^\bullet$** to **BIH**.

Mechanism for the entire photocatalytic CO_2RR

The mechanism for the entire photocatalytic CO_2RR is proposed in Fig. 14. PC **5**, which had extended absorption into the visible light region, was excited by the light of 400 nm, generating the singlet excited state (^{1}**5***). This excited state was characterized by a

deeply negative oxidation potential (E ($\mathbf{5}^{\bullet+}/{}^1\mathbf{5}^*$) = –2.65 V vs SCE)) and underwent ET to $\mathbf{BI}^+$ (E_{red} = –1.96 V vs SCE), resulting in the formation of $\mathbf{5}^{\bullet+}$ and $\mathbf{BI}^{\bullet}$. Subsequently, $\mathbf{5}^{\bullet+}$ (E_{red} = 0.34 V vs SCE) accepted an electron from $\mathbf{HA}^-$ (E_{ox} = 0.47 V vs SCE)[61] to regenerate **5** along with the formation of $\mathbf{HA}^{\bullet}$. This process was slightly endothermic. The HAT process from $\mathbf{HA}^-$ or $\mathbf{HA}^{\bullet}$ to $\mathbf{BI}^{\bullet}$ was effective (ΔH^o = –31.1 or –25.4 kcal/mol, respectively) in reducing $\mathbf{BI}^{\bullet}$ to **BIH**. The resultant **BIH** readily captured CO_2 under ambient conditions (1 atm CO_2, at 293 K) to produce $\mathbf{BI^+(HCOO^-)}$, according to a previous report.[34] In addition to CO_2 from the external source, CO_2 generated along with the conversion of **A** to **14** served as a carbon source for formate. Products **14** and **15** resulting from **A** could function similarly as $\mathbf{HA}^-$ and $\mathbf{HA}^{\bullet}$, respectively; thus, $\mathbf{H_2A}$ served as a four-electron reductant in this CO_2RR. A small amount of formate was obtained without $\mathbf{BI^+(I)^-}$ (Table 1, entry 7), deducing that the direct ET from ${}^1\mathbf{5}^*$ to CO_2 could also proceed slightly; however, it was a minor pathway because oxalate, a dimer of $CO_2^{\bullet-}$, was not detected as a product.[62] Formate often acts as an electron or hydrogen atom donor;[63,64] Therefore, the reverse reaction, that is, conversion from formate to CO_2, could occur during CO_2RR, which could deteriorate the reaction efficiency and quantum yield. Therefore, we irradiated a mixture of formate and $\mathbf{BI^+(I^-)}$ in the presence of **5** under argon purging conditions to check the reversibility of CO_2RR (Fig. S24). No **BIH** was detected in this reaction, indicating that the reverse reaction was negligible.

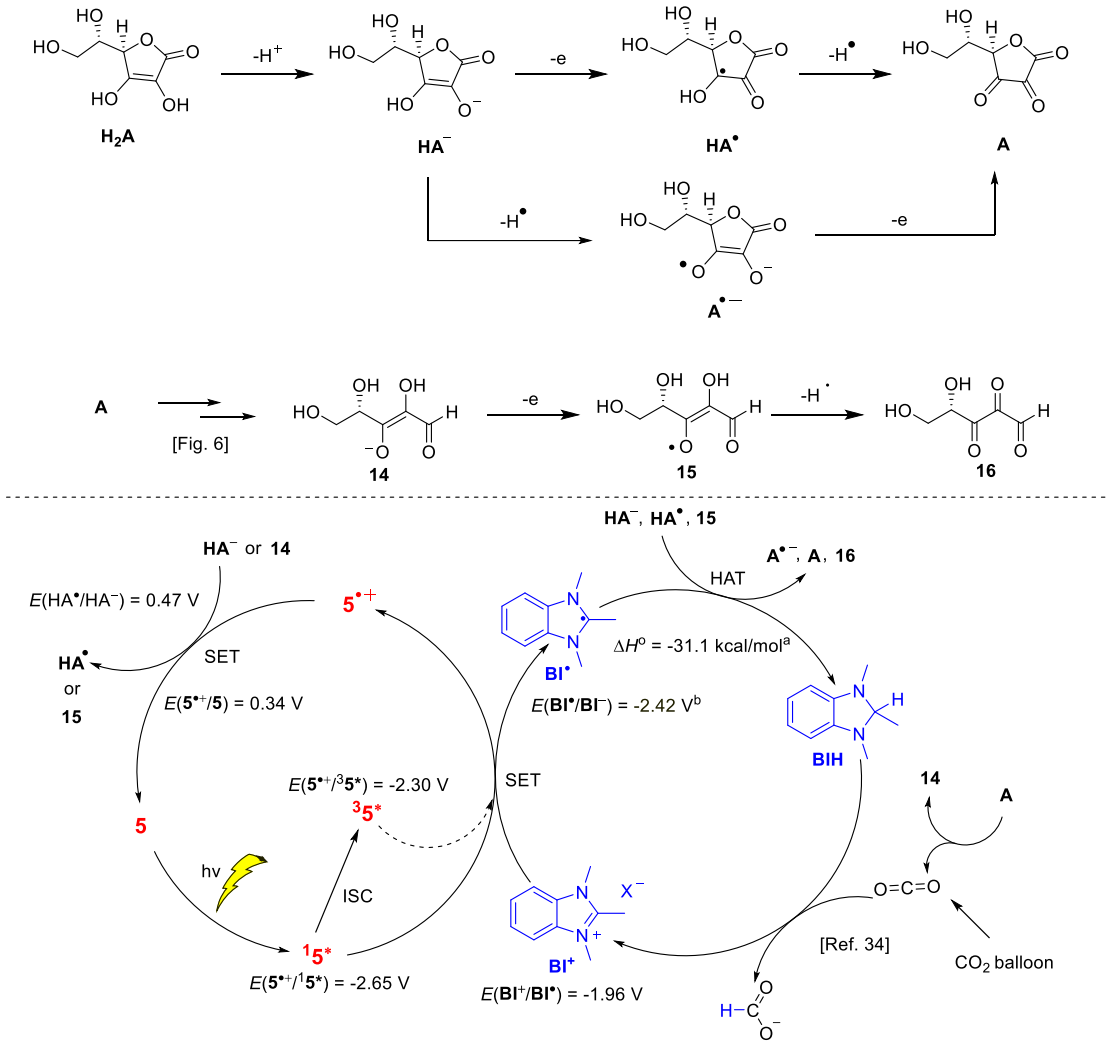

Figure 14. The proposed reaction mechanism for the photocatalytic CO_2RR. [a]Standard enthalpy change for the reaction (**BI•** + **HA**$^-$ → **BIH** + **A**$^{\bullet-}$) calculated using the density functional theory (DFT) method with (U)LC-BLYP/6-31++G(d)/CPCM(DMSO) basis sets. [b]Estimated value by the DFT calculation. Standard redox potentials are referred to saturated calomel electrode (SCE). ISC = intersystem crossing; HAT = hydrogen atom transfer; SET = single electron transfer.

In summary, the approach delineated in this study enables the transition metal-free photocatalytic CO_2RR with a high TON and TOF. The critical reaction is the photocatalytic regeneration of organohydrides with a high reduction capability. In the present system, high selectivity for the product formate is appealing and characteristic of using organohydride catalysts; the obvious drawback is the requirement of a sacrificial reductant. Thus, the coupling of the developed CO_2RR with the reaction system of the water oxidation without using transition metal catalysts is an attractive target for realizing artificial photosynthesis with water as a terminal reductant, an ongoing project in our laboratory.

Methods

General method for the photocatalytic CO_2RR (entry 1 in Table 1 as a representative example): A flame-dried 50-mL Schlenk tube with a Teflon cap and a magnetic stir bar was charged with **BI$^+$(I$^-$)** (7.2 mg, 0.025 mmol, 5 mol%), PC **1** (3.8 mg, 0.015 mmol, 3 mol%), ascorbic acid (88.1 mg, 0.500 mmol, 1.0 eq.), and K_2CO_3 (76.0 mg, 0.550 mmol, 1.1 eq.) Then, CH_3CN (8 mL) and distilled water (2 mL) were introduced into the mixture. The reaction mixture was degassed by three freeze–pump–thaw cycles. Subsequently, the reaction mixture was backfilled with CO_2 (>99.995% purity), and the CO_2 atmosphere was maintained using a balloon. The reaction was stirred under visible light irradiation (λ_{max} = 400 nm) for 4 h. After the reaction, 1,3,5-trimethyoxybenzene (40.6 mg) was added as an internal standard and distilled water (3 mL) was added to the resulting reaction mixture. Then, 0.6 mL of the solution was transferred to an NMR tube and subjected to ^{1}H NMR spectroscopic analysis using the solvent suppression technique. The yield of formate was 143% based on the ascorbic acid employed.

Data Availability

The data supporting the plots within this paper and other findings of this study, such as ^{1}H NMR and ^{13}C NMR spectra, cyclic voltammograms, experimental procedures, and quantum chemical calculations are available in the Supplementary Information.

Acknowledgments

Financial support from ENEOS TonenGeneral Research/Development Encouragement & Scholarship Foundation, Takahashi Industrial and Economic Research Foundation, The Takano Science Foundation, Kanamori Foundation, and Fukuoka Naohiko Memorial Foundation is greatly appreciated. We thank Ms. Tomoko Amimoto from the Natural Science Center for Basic Research and Development (N-BARD), Hiroshima University for the measurement of mass analysis. We thank Prof. Takashi Tachikawa and Dr. Zhujun Zhang in Kobe University for their help on GC analysis.

Author contributions

R.M. conceived and directed the project. R.M., W.X., and Y.K. wrote the paper. W.X., J.X., and U.M.I. performed most of the experiments under the supervision of R.M. and M.H. J.K., M.F., and Y.K. conducted transient absorption spectroscopy and fluorescence lifetime measurements. All the authors discussed the results and commented on the manuscript.

Competing interests

The authors declare no competing interests.

References

1 White, J. L. *et al.* Light-driven heterogeneous reduction of carbon dioxide: Photocatalysts and photoelectrodes. *Chem. Rev.* **115**, 12888-12935 (2015).

2 MacDowell, N. *et al.* An overview of CO_2 capture technologies. *Energy Environ. Sci.* **3**, 1645-1669 (2010).

3 Aresta, M., Dibenedetto, A. & Angelini, A. Catalysis for the valorization of

exhaust carbon: From CO_2 to chemicals, materials, and fuels. Technological use of CO_2. *Chem. Rev.* **114**, 1709-1742 (2014).

4 Ra, E. C. *et al.* Recycling carbon dioxide through catalytic hydrogenation: Recent key developments and perspectives. *ACS Catal.* **10**, 11318-11345 (2020).

5 Qiao, J., Liu, Y., Hong, F. & Zhang, J. A review of catalysts for the electroreduction of carbon dioxide to produce low-carbon fuels. *Chem. Soc. Rev.* **43**, 631-675 (2014).

6 Takeda, H., Cometto, C., Ishitani, O. & Robert, M. Electrons, photons, protons and earth-abundant metal complexes for molecular catalysis of CO_2 reduction. *ACS Catal.* **7**, 70-88 (2017).

7 Seyferth, D. The grignard reagents. *Organometallics* **28**, 1598-1605 (2009).

8 Seo, H., Liu, A. & Jamison, T. F. Direct β-selective hydrocarboxylation of styrenes with CO_2 enabled by continuous flow photoredox catalysis. *J. Am. Chem. Soc.* **139**, 13969-13972 (2017).

9 Seo, H., Katcher, M. H. & Jamison, T. F. Photoredox activation of carbon dioxide for amino acid synthesis in continuous flow. *Nat. Chem.* **9**, 453-456 (2017).

10 Matsuoka, S., Kohzuki, T., Pac, C. & Yanagida, S. Photochemical reduction of carbon dioxide to formate catalyzed by *p*-terphenyl in aprotic polar solvent. *Chem. Lett.* **19**, 2047-2048 (1990).

11 Matsuoka, S., Yamamoto, K., Pac, C. & Yanagida, S. Enhanced *p*-terphenyl-catalyzed photoreduction of CO_2 to co through the mediation of Co(III)–cyclam complex. *Chem. Lett.* **20**, 2099-2100 (1991).

12 Zhang, X., Cibian, M., Call, A., Yamauchi, K. & Sakai, K. Photochemical CO_2 reduction driven by water-soluble copper(I) photosensitizer with the catalysis accelerated by multi-electron chargeable cobalt porphyrin. *ACS Catal.* **9**, 11263-11273 (2019).

13 Tamaki, Y., Morimoto, T., Koike, K. & Ishitani, O. Photocatalytic CO_2 reduction with high turnover frequency and selectivity of formic acid formation using Ru(II) multinuclear complexes. *Proc. Natl Acad. Sci. USA* **109**, 15673-15678 (2012).

14 Lee, S. E. *et al.* Visible-light photocatalytic conversion of carbon dioxide by Ni(II) complexes with N_4S_2 coordination: Highly efficient and selective production of formate. *J. Am. Chem. Soc.* **142**, 19142-19149 (2020).

15 Liu, X., Inagaki, S. & Gong, J. Heterogeneous molecular systems for photocatalytic CO_2 reduction with water oxidation. *Angew. Chem. Int. Ed.* **55**, 14924-14950 (2016).

16 Tsujiguchi, T. *et al.* Acceleration of electrochemical CO_2 reduction to formate at the Sn/reduced graphene oxide interface. *ACS Catal.* **11**, 3310-3318 (2021).

17 Hietala, J. *et al.* in *Ullmann's encyclopedia of industrial chemistry* 7th edn (eds Bellussi, G. et al.) (2016); https://doi.org/10.1002/14356007.a12_013.pub3.

18 Yang, J. Y., Kerr, T. A., Wang, X. S. & Barlow, J. M. Reducing CO_2 to HCO_2^- at mild potentials: Lessons from formate dehydrogenase. *J. Am. Chem. Soc.* **142**, 19438-19445 (2020).

19 Lorenzo, B. F. & O'Kiely, P. Alternatives to formic acid as a grass silage additive under two contrasting ensilability conditions. *Irish J. Agr. Food Res.* **47**, 135-149 (2008).
20 Bahuguna, A. & Sasson, Y. Formate-bicarbonate cycle as a vehicle for hydrogen and energy storage. *ChemSusChem* **14**, 1258-1283 (2021).
21 Enthaler, S. Carbon dioxide—the hydrogen-storage material of the future? *ChemSusChem* **1**, 801-804 (2008).
22 Joó, F. Breakthroughs in hydrogen storage—formic acid as a sustainable storage material for hydrogen. *ChemSusChem* **1**, 805-808 (2008).
23 Boston, D. J., Xu, C., Armstrong, D. W. & MacDonnell, F. M. Photochemical reduction of carbon dioxide to methanol and formate in a homogeneous system with pyridinium catalysts. *J. Am. Chem. Soc.* **135**, 16252-16255 (2013).
24 Tamaki, Y., Koike, K. & Ishitani, O. Highly efficient, selective, and durable photocatalytic system for CO_2 reduction to formic acid. *Chem. Sci.* **6**, 7213-7221 (2015).
25 P, S. & Mandal, S. K. From CO_2 activation to catalytic reduction: A metal-free approach. *Chem. Sci.* **11**, 10571-10593 (2020).
26 Oh, Y. & Hu, X. Organic molecules as mediators and catalysts for photocatalytic and electrocatalytic CO_2 reduction. *Chem. Soc. Rev.* **42**, 2253-2261 (2013).
27 Lim, C.-H., Holder, A. M., Hynes, J. T. & Musgrave, C. B. Catalytic reduction of CO_2 by renewable organohydrides. *J. Phys. Chem. Lett.* **6**, 5078-5092 (2015).
28 Keith, J. A. & Carter, E. A. Theoretical insights into electrochemical CO_2 reduction mechanisms catalyzed by surface-bound nitrogen heterocycles. *J. Phys. Chem. Lett.* **4**, 4058-4063 (2013).
29 Alherz, A. *et al.* Renewable hydride donors for the catalytic reduction of CO_2: A thermodynamic and kinetic study. *J. Phys. Chem. B* **122**, 10179-10189 (2018).
30 Wen, F. *et al.* Amide-bridged conjugated organic polymers: Efficient metal-free catalysts for visible-light-driven CO_2 reduction with H_2O to CO. *Chem. Sci.* **12**, 11548-11553 (2021).
31 Wang, Y., Godin, R., Durrant, J. R. & Tang, J. Efficient hole trapping in carbon dot/oxygen-modified carbon nitride heterojunction photocatalysts for enhanced methanol production from CO_2 under neutral conditions. *Angew. Chem. Int. Ed.* **60**, 20811-20816 (2021).
32 Mazzanti, S. *et al.* All-organic Z-scheme photoreduction of CO_2 with water as the donor of electrons and protons. *Appl. Catal. B: Environ.* **285**, 119773 (2021).
33 Courtemanche, M.-A., Légaré, M.-A., Maron, L. & Fontaine, F.-G. A highly active phosphine–borane organocatalyst for the reduction of CO_2 to methanol using hydroboranes. *J. Am. Chem. Soc.* **135**, 9326-9329 (2013).
34 Lim, C.-H. *et al.* Benzimidazoles as metal-free and recyclable hydrides for CO_2 reduction to formate. *J. Am. Chem. Soc.* **141**, 272-280 (2019).
35 Rueping, M., Dufour, J. & Schoepke, F. R. Advances in catalytic metal-free reductions: From bio-inspired concepts to applications in the organocatalytic synthesis of pharmaceuticals and natural products. *Green Chem.* **13**, 1084-1105 (2011).

36 Lu, L.-Q., Li, Y., Junge, K. & Beller, M. Iron-catalyzed hydrogenation for the in situ regeneration of an NAD(P)H model: Biomimetic reduction of α-keto-/α-iminoesters. *Angew. Chem. Int. Ed.* **52**, 8382-8386 (2013).

37 Chen, Q.-A. *et al.* Dihydrophenanthridine: A new and easily regenerable NAD(P)H model for biomimetic asymmetric hydrogenation. *J. Am. Chem. Soc.* **134**, 2442-2448 (2012).

38 Chen, Q.-A. *et al.* Biomimetic asymmetric hydrogenation: In situ regenerable Hantzsch esters for asymmetric hydrogenation of benzoxazinones. *J. Am. Chem. Soc.* **133**, 16432-16435 (2011).

39 Paul, C. E., Arends, I. W. C. E. & Hollmann, F. Is simpler better? Synthetic nicotinamide cofactor analogues for redox chemistry. *ACS Catal.* **4**, 788-797 (2014).

40 Wu, H. *et al.* Methods for the regeneration of nicotinamide coenzymes. *Green Chem.* **15**, 1773-1789 (2013).

41 Ohtsu, H. & Tanaka, K. An organic hydride transfer reaction of a ruthenium NAD model complex leading to carbon dioxide reduction. *Angew. Chem. Int. Ed.* **51**, 9792-9795 (2012).

42 Emmanuel, M. A., Greenberg, N. R., Oblinsky, D. G. & Hyster, T. K. Accessing non-natural reactivity by irradiating nicotinamide-dependent enzymes with light. *Nature* **540**, 414-417 (2016).

43 Wang, J., Zhu, Z.-H., Chen, M.-W., Chen, Q.-A. & Zhou, Y.-G. Catalytic biomimetic asymmetric reduction of alkenes and imines enabled by chiral and regenerable NAD(P)H models. *Angew. Chem. Int. Ed.* **58**, 1813-1817 (2019).

44 Ohtsu, H. & Tanaka, K. Drastic difference in the photo-driven hydrogenation reactions of ruthenium complexes containing nad model ligands. *Chem. Commun.* **48**, 1796-1798 (2012).

45 Ma, B. *et al.* Efficient visible-light-driven CO_2 reduction by a cobalt molecular catalyst covalently linked to mesoporous carbon nitride. *J. Am. Chem. Soc.* **142**, 6188-6195 (2020).

46 Shon, J.-H. *et al.* Photoredox catalysis on unactivated substrates with strongly reducing iridium photosensitizers. *Chem. Sci.* **12**, 4069-4078 (2021).

47 Hong, D., Tsukakoshi, Y., Kotani, H., Ishizuka, T. & Kojima, T. Visible-light-driven photocatalytic CO_2 reduction by a Ni(II) complex bearing a bioinspired tetradentate ligand for selective CO production. *J. Am. Chem. Soc.* **139**, 6538-6541 (2017).

48 Kamada, K. *et al.* Photocatalytic CO_2 reduction using a robust multifunctional iridium complex toward the selective formation of formic acid. *J. Am. Chem. Soc.* **142**, 10261-10266 (2020).

49 Hasegawa, E. *et al.* Photoinduced electron transfer reactions of α,β-epoxy ketones with 2-phenyl-N,N-dimethylbenzimidazoline (PDBMI): Significant water effect on the reaction pathway. *Tetrahedron Lett.* **37**, 7079-7082 (1996).

50 Ilic, S., Alherz, A., Musgrave, C. B. & Glusac, K. D. Importance of proton-coupled electron transfer in cathodic regeneration of organic hydrides. *Chem. Commun.* **55**, 5583-5586 (2019).

51 Hasegawa, E. *et al.* Photoinduced electron-transfer systems consisting of electron-donating pyrenes or anthracenes and benzimidazolines for reductive transformation of carbonyl compounds. *Tetrahedron* **62**, 6581-6588 (2006).

52 Matsubara, R. *et al.* UVA- and visible-light-mediated generation of carbon radicals from organochlorides using nonmetal photocatalyst. *J. Org. Chem.* **83**, 9381-9390 (2018).

53 Yabuta, T., Hayashi, M. & Matsubara, R. Photocatalytic reductive C–O bond cleavage of alkyl aryl ethers by using carbazole catalysts with cesium carbonate. *J. Org. Chem.* **86**, 2545-2555 (2021).

54 Kimoto, E., Tanaka, H., Ohmoto, T. & Choami, M. Analysis of the transformation products of dehydro-L-ascorbic acid by ion-pairing high-performance liquid chromatography. *Anal. Biochem.* **214**, 38-44 (1993).

55 McClure, L. J. & Ford, P. C. Ligand macrocycle effects on the photophysical properties of rhodium(III) complexes: A detailed investigation of *cis*- and *trans*-dicyano(1,4,8,11-tetraazacyclotetradecane)rhodium(III) and related species. *J. Phys. Chem.* **96**, 6640-6650 (1992).

56 Ota, E., Wang, H., Frye, N. L. & Knowles, R. R. A redox strategy for light-driven, out-of-equilibrium isomerizations and application to catalytic C–C bond cleavage reactions. *J. Am. Chem. Soc.* **141**, 1457-1462 (2019).

57 Roth, H. G., Romero, N. A. & Nicewicz, D. A. Experimental and calculated electrochemical potentials of common organic molecules for applications to single-electron redox chemistry. *Synlett* **27**, 714-723 (2016).

58 Rehm, D. & Weller, A. Kinetics of fluorescence quenching by electron and H-atom transfer. *Isr. J. Chem.* **8**, 259-& (1970).

59 Connelly, N. G. & Geiger, W. E. Chemical redox agents for organometallic chemistry. *Chem. Rev.* **96**, 877-910 (1996).

60 Zhu, X.-Q., Mu, Y.-Y. & Li, X.-T. What are the differences between ascorbic acid and NADH as hydride and electron sources in vivo on thermodynamics, kinetics, and mechanism? *J. Phys. Chem. B* **115**, 14794-14811 (2011).

61 Macartney, D. H. & Sutin, N. The oxidation of ascorbic acid by tris(2,2′-bipyridine) complexes of osmium(III), ruthenium(III) and nickel(III) in aqueous media: Applications of the Marcus cross-relation. *Inorg. Chim. Acta* **74**, 221-228 (1983).

62 Ju, T. *et al.* Dicarboxylation of alkenes, allenes and (hetero)arenes with CO_2 via visible-light photoredox catalysis. *Nat. Catal.* **4**, 304-311 (2021).

63 Huang, Q., Wu, J.-W. & Xu, H.-J. Biomimetic hydrogenation: A reusable nadh co-enzyme model for hydrogenation of α,β-epoxy ketones and 1,2-diketones. *Tetrahedron Lett.* **54**, 3877-3881 (2013).

64 Lo, H. C., Buriez, O., Kerr, J. B. & Fish, R. H. Regioselective reduction of NAD^+ models with $[Cp^*Rh(bpy)H]^+$: Structure–activity relationships and mechanistic aspects in the formation of the 1,4-NADH derivatives. *Angew. Chem. Int. Ed.* **38**, 1429-1432 (1999).